

Corbino magnetoresistance in neutral graphene

Vanessa Gall,^{1,2} Boris N. Narozhny,^{2,3} and Igor V. Gornyi^{1,2,4}

¹*Institute for Quantum Materials and Technologies, Karlsruhe Institute of Technology, 76021 Karlsruhe, Germany*

²*Institut für Theorie der Kondensierten Materie, Karlsruhe Institute of Technology, 76128 Karlsruhe, Germany*

³*National Research Nuclear University MEPhI (Moscow Engineering Physics Institute), 115409 Moscow, Russia*

⁴*Ioffe Institute, 194021 St. Petersburg, Russia*

(Dated: May 30, 2023)

We explore the magnetohydrodynamics of Dirac fermions in neutral graphene in the Corbino geometry. Based on the fully consistent hydrodynamic description derived from a microscopic framework and taking into account all peculiarities of graphene-specific hydrodynamics, we report the results of a comprehensive study of the interplay of viscosity, disorder-induced scattering, recombination, energy relaxation, and interface-induced dissipation. In the clean limit, magnetoresistance of a Corbino sample is determined by viscosity. Hence the Corbino geometry could be used to measure the viscosity coefficient in neutral graphene.

Transport measurements remain one of the most common experimental tools in condensed matter physics. Having dramatically evolved past the original task of establishing bulk material characteristics such as electrical and thermal conductivities, modern experiments often involve samples that are tailor-made to target particular properties or behavior.

In recent years considerable efforts have been devoted to uncovering the collective or hydrodynamic flows of charge carriers in ultraclean materials as predicted theoretically [1–4]. Several dedicated experiments focused on answering two major questions: is the observed electronic flow really hydrodynamic and how to measure electronic viscosity [5–10], the quantity that fascinates physicists beyond the traditional condensed matter physics [11–18]. The hydrodynamic regime is apparently easiest to achieve in graphene [2–4]. This material is especially interesting since it can host two drastically different types of hydrodynamic behavior: (i) “conventional” at relatively high carrier densities [3, 19, 20] and (ii) “unconventional” at charge neutrality [21, 22].

Linearity of the excitation spectrum in graphene leads to the fact that electronic momentum density defines the energy current, \mathbf{j}_E . In the intermediate temperature window where electron-electron interaction is the dominant scattering process in the system ($\ell_{ee} \ll \ell_{dis}, \ell_{e-ph}, W$, in the self-evident notation) the energy flow becomes hydrodynamic. At high carrier densities (in “doped graphene”) the energy current is essentially equivalent to the electric current, \mathbf{j} , allowing one to formulate a Navier-Stokes-like equation for \mathbf{j} [20] as pioneered by Gurzhi [19].

At charge neutrality and in the absence of the external magnetic field ($\mathbf{B} = 0$) the energy and electric currents decouple [23]. In the hydrodynamic regime the electric current remains Ohmic [22] (with the “internal” or “quantum” conductivity σ_Q due to electron-electron interaction [24–27]), while the Navier-Stokes-like equation describes the energy current [22, 28, 29]. If external magnetic field is applied, the energy and charge flows become entangled [21–23] allowing for a possibility to detect the hydrodynamic flow in electronic transport experiments. In particular, a bulk (infinite) system is characterized

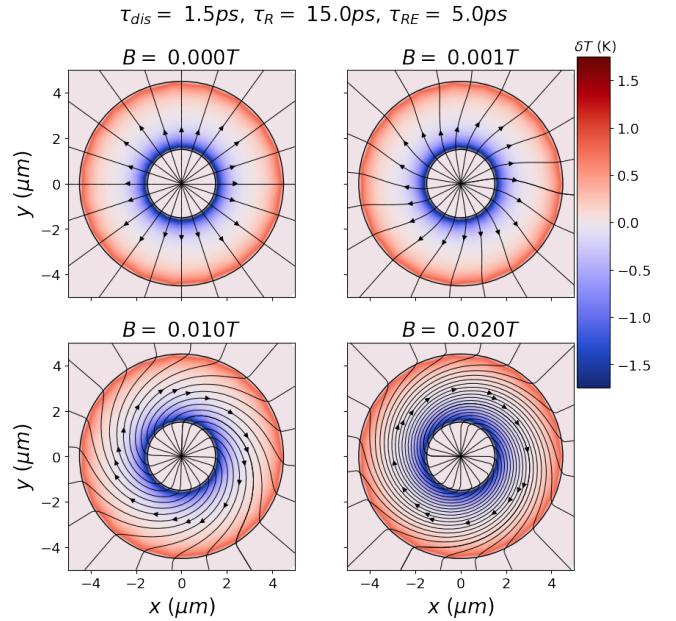


FIG. 1. Hydrodynamic velocity \mathbf{u} and temperature δT distribution in the device obtained by solving the hydrodynamic equations at relatively high temperatures where energy relaxation is dominated by supercollisions. Arrows indicate \mathbf{u} and the color map shows δT . The quantitative results were computed using the following values of the average temperature $T = 150$ K, disorder scattering time $\tau_{dis} = 1.5$ ps (corresponding to the scattering rate $\tau_{dis}^{-1} \approx 0.67$ THz ≈ 5.1 K), recombination time $\tau_R = 15$ ps, energy relaxation time $\tau_{RE} = 5$ ps, dimensionless coupling constant in graphene $\alpha = 0.5$, carrier density in the leads $n_L = 5 \times 10^{12}$ cm $^{-2}$, and the current passing through the device $I = 1$ μ A. The four panels correspond to the indicated values of magnetic field.

by positive, parabolic magnetoresistance [23, 30] proportional to the disorder mean free time τ_{dis} (disorder scattering is the only mechanism of momentum relaxation).

The outcome of a given measurement is strongly influenced by the sample size and geometry. Early experiments focused on either the “strip” (or Hall bar) [5–8] or

the point contact geometry [9, 10], while more recently data on Corbino disks became available [31].

The simplest viscous phenomenon one can look for in a long (striplike) sample [7–10, 12, 32–52] is the Poiseuille flow [53–55]. This flow is characterized by a parabolic velocity profile with the curvature determined by viscosity. In doped graphene the Poiseuille flow of charge can be detected by imaging the electric current density [8]. In contrast, neutral graphene exhibits the Poiseuille flow of the energy current [56]. Moreover, at relatively high temperatures where hydrodynamic behavior in graphene is observed the electron-phonon interaction (either direct [23, 57, 58] or via “supercollisions” [59–64]) cannot be neglected and hence electronic energy is not conserved. The resulting energy relaxation dwarfs the viscous contribution to the Navier-Stokes [65] equation.

Applying a perpendicular magnetic field to a neutral graphene strip leads to a coupled charge and energy flow with the two currents being orthogonal [23]. The electric current flowing along the strip is accompanied by a neutral quasiparticle flow in the lateral direction resulting in energy and quasiparticle accumulation near the strip boundaries [66, 67]. The accumulation is limited by quasiparticle recombination [67] and energy relaxation processes [59]. As a result, the boundary region’s contribution to the resistance is linear in the applied magnetic field [23, 48, 67, 68], in contrast to the standard quadratic magnetoresistance of the bulk system [23, 30]. In classically strong fields the boundary contribution dominates making the linear magnetoresistance directly observable. This effect is not specific to Dirac fermions as shown by experiments in bilayer graphene [69].

The Corbino geometry presents an interesting alternative to the Hall bar experiments [31, 65, 70–78]. In a typical measurement the electric current is passed from the inner to the outer boundary of a Corbino disk. The specific feature of the stationary flow in this geometry is that the magnitude of the radial component of the current is determined by the continuity equation alone. In the absence of the magnetic field the whole current flows radially. Combining the solution of the continuity equation with the hydrodynamic Gurzhi equation (e.g., in doped graphene) leads to an apparent paradox [73]: the current flow appears unaffected by viscosity. However, the dissipated energy is still determined by viscosity leading to the jumps of electric potential at the contacts thus resolving the paradox. In a perpendicular magnetic field the system exhibits parabolic magnetoresistance inverse proportional to the viscosity and independent of the disorder scattering. Applied phenomenologically to neutral graphene (neglecting contact effects) [78] this conclusion stands in sharp contrast to the standard result [23, 30] raising the question of the fate of the disorder-limited bulk magnetoresistance in the Corbino geometry.

In this paper we investigate hydrodynamic flows in neutral graphene in the Corbino disk subjected to the perpendicular magnetic field based on the graphene-specific hydrodynamic theory [2, 22, 59] reporting the

results of a careful study of the interplay of viscosity, disorder-induced scattering, recombination, energy relaxation, and interface-induced dissipation. Solving the hydrodynamic equations we find the spatial distribution of the hydrodynamic velocity \mathbf{u} , temperature (see Fig. 1), electric current, and potential φ (see Fig. 2). Furthermore, we calculate the field-dependent resistance of the whole Corbino sample including the leads. Keeping in mind recent and ongoing experiments, it appears logical to include the effect of the lead resistance in order to achieve a more realistic description of the Corbino device. However, the theoretical limit of “ideal” leads can be considered without any complications.

The main results of this paper are as follows. We show that magnetoresistance of the Corbino device exhibits a crossover from the “hydrodynamic” (viscosity-dominated) to the “bulk” (disorder-limited) behavior with the increasing system size as compared to the Gurzhi length $\ell_G = \sqrt{\nu\tau_{\text{dis}}}$ [46–49, 52] (ν is the kinematic viscosity [3, 5, 6, 55, 79] and τ_{dis} is the disorder mean free time). In the clean limit ($\tau_{\text{dis}} \rightarrow \infty$) magnetoresistance remains finite and is determined by viscosity offering a way to measure the viscosity coefficient in neutral graphene. In classically strong fields magnetoresistance remain parabolic (in contrast to the linear magnetoresistance in the strip geometry). The “contact magnetoresistance” induced through the dissipation jump is present, but is typically weaker than the bulk contribution.

I. MAGNETOHYDRODYNAMICS IN GRAPHENE

Our arguments are based on the hydrodynamic theory of electronic transport in neutral graphene derived from the kinetic (Boltzmann) equation [21, 22, 59] or from the microscopic Keldysh technique [80]. At charge neutrality both bands contribute to transport on equal footing. A current-carrying state is characterized by the chemical potentials μ_{\pm} of each band or by their linear combinations [22, 81]

$$\mu = \frac{\mu_+ + \mu_-}{2}, \quad \mu_I = \frac{\mu_+ - \mu_-}{2}, \quad (1a)$$

conjugate to the “charge” and “imbalance” (or “total quasiparticle”) densities

$$n = n_+ - n_-, \quad n_I = n_+ + n_-. \quad (1b)$$

In equilibrium $\mu_I = 0$. Any macroscopic current can be expressed as a product of the corresponding density and hydrodynamic velocity \mathbf{u} (up to dissipative corrections). Due to the kinematic peculiarity of the Dirac fermions in graphene known as the “collinear scattering singularity” [21, 25] one has to consider the electric, energy, and imbalance, \mathbf{j}_I currents defined as

$$\mathbf{j} = n\mathbf{u} + \delta\mathbf{j}, \quad \mathbf{j}_I = n_I\mathbf{u} + \delta\mathbf{j}_I, \quad \mathbf{j}_E = W\mathbf{u}, \quad (2)$$

where \mathcal{W} is the enthalpy density and $\delta\mathbf{j}$ and $\delta\mathbf{j}_I$ are the dissipative corrections. In the degenerate limit $\mu \gg T$ the dissipative corrections vanish [22, 28] justifying the applicability of the single-band picture to doped graphene. At charge neutrality $n = 0$, the electric and energy currents in Eq. (2) appear to be decoupled [22].

Within linear response, steady-state macroscopic currents obey the linearized hydrodynamic equations [82]. Assuming that the dominant mechanism of energy relaxation is supercollisions [59], the equations have the form

$$\nabla \cdot \delta\mathbf{j} = 0, \quad (3a)$$

$$n_I \nabla \cdot \mathbf{u} + \nabla \cdot \delta\mathbf{j}_I = -\frac{12 \ln 2}{\pi^2} \frac{n_I \mu_I}{T \tau_R}, \quad (3b)$$

$$\nabla \delta P = \eta \Delta \mathbf{u} + \frac{e}{c} \delta\mathbf{j} \times \mathbf{B} - \frac{3P\mathbf{u}}{v_g^2 \tau_{\text{dis}}}, \quad (3c)$$

$$3P \nabla \cdot \mathbf{u} = -\frac{2\delta P}{\tau_{RE}}. \quad (3d)$$

Here Eq. (3a) is the continuity equation; Eq. (3b) is the ‘‘imbalance’’ continuity equation [22, 81] (where v_g is the band velocity in graphene, c is the speed of light, e is the unit charge, and τ_R is the recombination time); Eq. (3c) is the linearized Navier-Stokes equation [22, 29, 82, 83] (with η being the shear viscosity); and Eq. (3d) is the linearized ‘‘thermal transport’’ equation (τ_{RE} is the energy relaxation time [59]). We follow the standard approach [55] where the thermodynamic quantities are replaced by the corresponding equilibrium functions of the hydrodynamic variables. Equilibrium thermodynamic quantities, i.e., the pressure $P = 3\zeta(3)T^3/(\pi v_g^2)$, enthalpy density \mathcal{W} , imbalance density, $n_I = \pi T^2/(3v_g^2)$, and energy density are related by the ‘‘equation of state’’, $\mathcal{W} = 3P = 3n_E/2$. Equations (3) should be solved for the unknowns \mathbf{u} , μ_I , and δP keeping the remaining (thermodynamic) quantities, e.g., n_I , P , and T , constant.

The dissipative corrections to the macroscopic currents can be determined from the underlying microscopic theory [22, 29, 82] and are expressed in terms of the same variables closing the set of hydrodynamic equations (3)

$$\delta\mathbf{j} = \frac{1}{e^2 \tilde{R}} \left[e\mathbf{E} + \omega_B \mathbf{e}_B \times \left(\frac{\alpha_1 \delta_I \nabla \mu_I}{\tau_{\text{dis}}^{-1} + \delta_I^{-1} \tau_{22}^{-1}} - \frac{2T \ln 2}{v_g^2} \mathbf{u} \right) \right], \quad (4a)$$

$$\delta\mathbf{j}_I = -\frac{\delta_I}{\tau_{\text{dis}}^{-1} + \delta_I^{-1} \tau_{22}^{-1}} \frac{1}{e^2 \tilde{R}} \times \left[\alpha_1 \omega_B \mathbf{e}_B \times \mathbf{E} + \frac{2T \ln 2}{\pi} e^2 R_0 \nabla \mu_I + \alpha_1 \omega_B^2 \frac{2T \ln 2}{v_g^2} \mathbf{u} \right], \quad (4b)$$

$$\tilde{R} = R_0 + \alpha_1^2 \delta_I \tilde{R}_B. \quad (4c)$$

In Eqs. (4) the following notations are introduced. R_0 is the zero-field bulk resistivity in neutral graphene [23, 30]

$$R_0 = \frac{\pi}{2e^2 T \ln 2} \left(\frac{1}{\tau_{11}} + \frac{1}{\tau_{\text{dis}}} \right) \xrightarrow{\tau_{\text{dis}} \rightarrow \infty} \frac{1}{\sigma_Q}, \quad (5)$$

where $\tau_{11} \propto \alpha_g^{-2} T^{-1}$ describes the appropriate electron-electron collision integral. \tilde{R}_B denotes [65, 82]

$$\tilde{R}_B = \frac{\pi}{2e^2 T \ln 2} \frac{\omega_B^2}{\tau_{\text{dis}}^{-1} + \delta_I^{-1} \tau_{22}^{-1}}, \quad (6)$$

where $\tau_{22} \propto \alpha_g^{-2} T^{-1}$ describes a component of the collision integral that is qualitatively similar, but quantitatively distinct from τ_{11} and $\delta_I \approx 0.28$. Another numerical factor in Eqs. (4) is $\alpha_1 \approx 2.08$ and $\omega_B = eBv_g^2/(2cT \ln 2)$ is the generalized cyclotron frequency at $\mu = 0$.

The shear viscosity at charge neutrality and in the absence of magnetic field was evaluated in Refs. [22, 79, 83] and has the form

$$\eta(\mu = 0, B = 0) = \mathcal{B} \frac{T^2}{\alpha_g^2 v_g^2}, \quad \mathcal{B} \approx 0.45. \quad (7)$$

Within the renormalization group (RG) approach, α_g is a running coupling constant [56, 83–86]. However, the product $\alpha_g v_g$ remains constant along the RG flow [24, 83]. Hence Eq. (7) gives the correct form of shear viscosity in neutral graphene [84]. Within the kinetic theory approach, the coefficient \mathcal{B} can be expressed in terms of time scales characterizing the collision integral [22, 79]. At neutrality these time scales are qualitatively similar to, but quantitatively distinct from τ_{11} and τ_{22} . The similarity follows from the fact that in general all time scales are functions of the chemical potential and temperature [22, 28, 87]. At neutrality $\mu = 0$ and hence all time scales are inverse proportional to temperature.

As a function of the magnetic field, the viscosity coefficient in neutral graphene exhibit a weak decay until eventually saturating in classically strong fields [79]

$$\eta(\mu = 0, B) = \frac{\mathcal{B} + \mathcal{B}_1 \gamma_B^2}{1 + \mathcal{B}_2 \gamma_B^2} \frac{T^2}{\alpha_g^2 v_g^2}, \quad \gamma_B = \frac{|e| v_g^2 B}{\alpha_g^2 c T^2}, \quad (8)$$

where

$$\mathcal{B}_1 \approx 0.0037, \quad \mathcal{B}_2 \approx 0.0274.$$

This behavior should be contrasted with the more conventional Lorentzian decay of field-dependent shear viscosity in doped graphene [6, 45, 46, 79, 88]. However, in weak fields where most present-day experiments are performed this distinction is negligible. Moreover, due to the smallness of the coefficient \mathcal{B}_1 and \mathcal{B}_2 we disregard the field dependence of η in what follows.

Under the assumptions of the hydrodynamic regime, disorder scattering is characterized by the large mean free time, $\tau_{\text{dis}} \gg \tau_{11}, \tau_{22}$, yielding a negligible contribution to Eqs. (5) and (6). Equation (5) describes the uniform bulk current (at $\mathbf{B} = 0$) and is independent of viscosity (i.e., in a channel [3, 21, 67, 82]). In contrast, in the Corbino geometry the current flow is necessarily inhomogeneous and hence viscous dissipation must be taken into account.

II. BOUNDARY CONDITIONS

Differential equations (3) should be supplemented by boundary conditions, which should be expressed in terms of the hydrodynamic velocity and macroscopic currents. The statement of the boundary conditions does not imply the validity of the hydrodynamic approximation at the sample edges and generally have to be derived from the underlying microscopic theory. However some of the boundary conditions can be derived based on the conservation laws alone. In the circular Corbino geometry conservation laws can be used to establish boundary conditions for radial components of the currents [65].

A. Radial components of macroscopic currents

A typical experimental setup involves a graphene sample (in our case, at charge neutrality) in the shape of an annulus placed between the inner (a disk of radius r_1) and outer (a ring with the inner radius r_2) metallic contacts (leads). The electric current I is injected into the center of the inner lead preserving the rotational invariance (e.g., through a thin vertical wire attached to the center point) and spreads towards the outer lead, which for concreteness we assume to be grounded. The overall voltage drop U is measured between two points in the two leads (at the radii $r_{\text{in}} < r_1$ and $r_{\text{out}} > r_2$) yielding the device resistance, $R = U/I$. The only boundaries in the system are between the sample and the external leads.

For simplicity, we assume both leads to be of the same material with a single-band electronic system, e.g., highly doped graphene with the same doping level. In that case, all macroscopic currents in the leads are proportional to the drift velocity and hence are determined by the injected current. In the stationary case, the continuity equation (3a) determines the radial component of the electric current density. In the inner lead this yields $j_r^{\text{in}} = I/(2\pi er)$, defining the radial component of the drift velocity, $u_r^{\text{in}} = j_r^{\text{in}}/n_L$ (n_L is the carrier density in the inner lead). Assuming charge conservation is not violated at the interface, we find the boundary condition between the inner lead and the sample

$$j_r(r_1 - \epsilon) = n_L u_r(r_1 - \epsilon) = \delta j_r(r_1 + \epsilon), \quad (9a)$$

where $\epsilon > 0$ is infinitesimal and we took into account that in neutral ($n = 0$) graphene $\mathbf{j} = \delta \mathbf{j}$.

The second hydrodynamic equation, Eq. (3b), is the continuity equation for the imbalance density. Although the total quasiparticle number is not conserved, integrating this equation over an infinitesimally thin region encompassing the boundary yields a similar boundary condition for the imbalance current assuming that the relaxation rate due to quasiparticle recombination is not singular at the boundary

$$j_{I,r}(r_1 - \epsilon) = n_L u_r(r_1 - \epsilon) = n_L u_r(r_1 + \epsilon) + \delta j_{I,r}(r_1 + \epsilon). \quad (9b)$$

Here we took into account the fact that in a single-band system \mathbf{j}_I is identical with \mathbf{j} .

Finally, Eq. (3d) is the linearized continuity equation for the entropy density (here we follow the standard practice [55] of replacing the continuity equation for the energy density by the entropy flow equation, also known as the thermal transport equation). Again, assuming the energy relaxation rate is not singular at the interface (i.e., the current flow is not accompanied by energy or excess heat accumulation at the boundary between the sample and the contact) we integrate Eq. (3d) over an infinitesimally thin region encompassing the boundary and arrive at the boundary condition for the entropy current

$$s^{\text{in}} u_r(r_1 - \epsilon) = s u_r(r_1 + \epsilon), \quad (9c)$$

where s and s^{in} are the entropy densities in the sample and inner lead, respectively.

B. Tangential flows in external magnetic field

The above boundary conditions (and the corresponding conditions on the outer lead) are sufficient to solve the hydrodynamic equations in the absence of magnetic field where all currents are radial [65]. An external magnetic field induces the tangential components of the currents due to the classical Hall effect. The continuity equations do not determine the tangential components and hence the boundary conditions have to be derived from a microscopic theory. Generally speaking, the boundary conditions depend on the presence of tangential forces at the interface, usually associated with edge roughness. Typically [2–4, 55, 73], one considers the two limiting cases of either the “no-slip” or “no-stress” boundary conditions corresponding to either the presence or the absence of the drag-like friction across the interface.

For contact interfaces in the Corbino geometry, the boundary conditions corresponding to the above limiting cases differ from the well-known expression of conventional hydrodynamics. The no-slip boundary condition now means that the tangential component of the hydrodynamic velocity is continuous across the interface (written as above for the inner interface)

$$u_{L,\vartheta}(r_1 - \epsilon) = u_{\vartheta}(r_1 + \epsilon), \quad (10a)$$

in contrast to the common condition of vanishing velocity at the channel boundary (the two are consistent, since in the latter case there is no flow beyond the edge).

The no-stress boundary condition means the absence of any forces along the interface in which case the tangential component of the stress tensor Π^{ij} is continuous. In polar coordinates appropriate for the Corbino geometry one finds

$$\Pi_{L,E}^{\vartheta r}(r_1 - \epsilon) = \Pi_E^{\vartheta j}(r_1 + \epsilon), \quad (10b)$$

The no-stress boundary condition is easy to derive starting from the kinetic equation. Multiplying the kinetic

equation by the momentum and summing over all quasi-particle states, one finds an equation featuring the gradient of the stress tensor [22] as well as macroscopic forces in the system. Now the boundary condition can be obtained by integrating that equation over the small volume around the interface. Unless there is a force localized at the interface (with a δ -function-like coordinate dependence on the hydrodynamic scale), this procedure would yield Eq. (10b). Usually, the interfaces are microscopically rough with the roughness providing such a force. As a result, the no-slip boundary condition is more commonly used. In neutral graphene, however, the quasiparticle wavelength typically exceeds any length scale associated with edge roughness leading to specular scattering [82] and Eq. (10b).

In the case of the hard wall edges, the boundary conditions were previously studied theoretically in Ref. [89] and confirmed experimentally in Ref. [8] where a nonzero slip length was proposed indicating a more general Maxwell's boundary condition. However, the specific choice of the boundary conditions does not lead to qualitatively different results [73]. Here we follow the hydrodynamic tradition and consider both the no-slip and no-stress boundary conditions.

C. Interface-induced dissipation and jumps of the electric potential

The hydrodynamic theory discussed so far completely describes the energy flow in neutral graphene. In order to establish the device resistance R we have to find the behavior of the electrochemical potential at the interfaces.

The standard description of interfaces between metals or semiconductors in terms of the contact resistance [90] can be carried over to neutral graphene [81]. In graphene, the contact resistance was recently measured in Ref. [8] (see also Refs. [31, 91, 92]). In the diffusive (or Ohmic) case, the contact resistance leads to a voltage drop that is small compared to that in the bulk of the sample and can be neglected. In contrast, in the ballistic case with almost no voltage drop in the bulk, most energy is dissipated at the contacts. Both scenarios neglect interactions.

In the diffusive regime interactions give rise to perturbative corrections to the bulk resistivity [93, 94] and the contact resistance can still be neglected. In ballistic samples electron-electron interaction may lead to the “Knudsen-Poiseuille” crossover [19] and drive the system to the hydrodynamic regime. In this case the Ohmic resistivity of the electronic fluid may remain small, but there exist other channels for dissipation due to viscosity [73] and energy relaxation processes [59]. In neutral graphene the effect is subtle [65], since the electric current is decoupled from the hydrodynamic energy flow. However, both are induced by the current source that provides the energy dissipated through all the above channels. The energy dissipated in the system corresponds to the overall voltage drop. In the bulk of the sample the

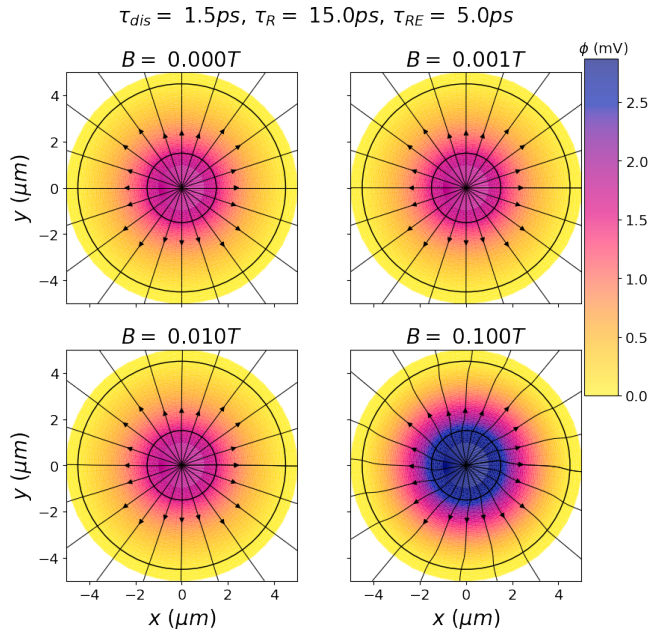


FIG. 2. Electric current density \mathbf{j} and potential ϕ in the device obtained by solving the hydrodynamic equations at relatively high temperatures where energy relaxation is dominated by supercollisions. Arrows indicate \mathbf{j} and the color map shows ϕ . The outer lead is chosen to be grounded. The four panels correspond to the indicated values of magnetic field. For the values of other parameters, see Fig 1.

voltage drop is Ohmic as determined by Eq. (4a), while the additional contribution takes the form of a potential jump at the interface between the sample and leads. At the same time, an excess electric field is induced in a thin Knudsen layer around the interface [73].

The magnitude of the jump in ϕ can be established by considering the flow of energy through the interface as suggested in Ref. [73] and detailed in neutral graphene at $B = 0$ in Ref. [65]. Consider the kinetic energy defined by integrating the energy density $n_E(\mathbf{u}) - n_E(0)$ over the volume

$$\mathcal{E} = \int dV [n_E(\mathbf{u}) - n_E(0)] \approx \int dV \frac{6P}{v_g^2} u^2, \quad (11)$$

which we have expanded to the leading order in \mathbf{u} (and hence in I). In the stationary state, dissipation is balanced by the work done by the source, such that the time derivative of the kinetic energy vanishes, $\mathcal{A} = \dot{\mathcal{E}} = 0$. Using the equations of motion and continuity equations to find time derivatives, one may split \mathcal{A} into the “bulk” and “boundary” contributions, $\mathcal{A} = \mathcal{A}_{\text{bulk}} + \mathcal{A}_{\text{edge}}$. The former may be interpreted as the bulk dissipation, while $\mathcal{A}_{\text{edge}}$ must include the energy brought in (carried away) through the boundary by the incoming (outgoing) flow. The boundary condition is then found under the assumption that energy is not accumulated at the interface.

Assuming the leads' material is highly doped graphene, the equation of motion is the usual Ohm's law where we

may combine the diffusion term [95] with a contribution of viscosity η_L due to disorder [96] into the gradient of the stress-energy tensor [23] and hence

$$\begin{aligned} \frac{3P_L}{v_g^2} \mathbf{u}_L \partial_t \mathbf{u}_L &= \\ &= u_L^i \left(-\frac{3P_L}{v_g^2} \frac{u_L^i}{\tau_L} - \nabla^j \Pi_{L,E}^{ij} + n_L e E^i + \frac{e}{c} \epsilon^{ijk} j^j B^k \right) \\ &= -\frac{3P_L}{v_g^2} \frac{u_L^2}{\tau_L} + \frac{\partial u_{L,i}}{\partial x_j} \Pi_{L,E}^{ij} + \frac{e}{c} \mathbf{u}_L \cdot (\mathbf{j} \times \mathbf{B}) + e\varphi \nabla \cdot \mathbf{j} \\ &\quad - \nabla^i \left(u_L^j \Pi_{L,E}^{ij} + e j^i \varphi \right). \end{aligned}$$

The last term in this expression determines the boundary contribution. Given that the Lorentz force does not explicitly contribute, the only difference from the expression derived in Ref. [65] at $\mathbf{B} = 0$ is the nonzero tangential components of the hydrodynamic velocity and the stress tensor (vanishing in the absence of magnetic field). In neutral graphene, we obtain a similar expression from the Navier-Stokes equation, while the Joule heat is determined by $\delta \mathbf{j}$. Equating the two contributions we find the jump of the potential in the form

$$\begin{aligned} \varphi(r_1 - \varepsilon) - \varphi(r_1 + \varepsilon) &= IR_c + \\ &+ \frac{2\pi r_1}{I} \left[(u_r \Pi_E^{rr} + u_\vartheta \Pi_E^{\vartheta r}) \Big|_{r_1+\varepsilon} \right. \\ &\quad \left. - (u_r \Pi_{L,E}^{rr} + u_\vartheta \Pi_{L,E}^{\vartheta r}) \Big|_{r_1-\varepsilon} \right], \end{aligned} \quad (12)$$

where R_c is the usual contact resistance [81]. A similar condition holds at the boundary with the outer lead.

III. HYDRODYNAMIC FLOWS IN THE CORBINO GEOMETRY

In polar coordinates and taking into account radial symmetry, the hydrodynamic equations (3) and (4) form two disjoint sets of differential equations. The first one determines the tangential component of the velocity u_ϑ :

$$\frac{1}{r} \frac{\partial(r\delta j_r)}{\partial r} = 0, \quad (13a)$$

$$\eta \partial_r \left(\frac{1}{r} \frac{\partial(r u_\vartheta)}{\partial r} \right) - \frac{eB}{c} \delta j_r - \frac{3P u_\vartheta}{v_g^2 \tau_{\text{dis}}} = 0, \quad (13b)$$

$$\delta j_r = \frac{1}{e^2 \tilde{R}} \left[e E_r(r) + \omega_B \frac{2T \ln 2}{v_g^2} u_\vartheta \right], \quad (13c)$$

$$\delta j_{I\vartheta} = -\frac{\alpha_1 \delta_I \omega_B}{\tau_{\text{dis}}^{-1} + \delta_I^{-1} \tau_{22}^{-1}} \delta j_r, \quad (13d)$$

while the second one involves the radial component u_r :

$$\frac{n_I}{r} \frac{\partial(r u_r)}{\partial r} + \frac{1}{r} \frac{\partial(r \delta j_{I r})}{\partial r} = -\frac{12 \ln 2}{\pi^2} \frac{n_I \mu_I(r)}{T \tau_R}, \quad (14a)$$

$$\frac{\partial \delta P}{\partial r} = \eta \partial_r \left(\frac{1}{r} \frac{\partial(r u_r)}{\partial r} \right) + \frac{eB}{c} \delta j_\vartheta - \frac{3P u_r}{v_g^2 \tau_{\text{dis}}}, \quad (14b)$$

$$\frac{3P}{r} \frac{\partial(r u_r)}{\partial r} = -\frac{2\delta P(r)}{\tau_{RE}}. \quad (14c)$$

$$\delta j_\vartheta = \frac{\omega_B}{e^2 \tilde{R}} \left(\frac{\alpha_1 \delta_I}{\tau_{\text{dis}}^{-1} + \delta_I^{-1} \tau_{22}^{-1}} \frac{\partial \mu_I}{\partial r} - \frac{2T \ln 2}{v_g^2} u_r \right), \quad (14d)$$

$$\delta j_{I r} = -\frac{2\delta_I T \ln 2}{\tau_{\text{dis}}^{-1} + \delta_I^{-1} \tau_{22}^{-1}} \left[\frac{R_0}{\pi \tilde{R}} \frac{\partial \mu_I}{\partial r} + \frac{\alpha_1 \omega_B^2}{e^2 \tilde{R}} \frac{u_r}{v_g^2} \right]. \quad (14e)$$

A. Tangential component of the velocity and bulk voltage drop

The bulk magnetoresistance can be found by solving Eqs. (13) with the appropriate boundary conditions. Combining Eqs. (13a) and (13b) we find an inhomogeneous Bessel equation for the tangential component of the velocity u_ϑ with the characteristic length scale being the Gurzhi length $\ell_G^2 = \eta v_g^2 \tau_{\text{dis}} / (3P)$. The boundary condition for u_ϑ is determined by microscopic details of viscous drag at the interface and hence is not universal. Here we follow the hydrodynamic tradition and consider both the no-slip and the no-stress boundary conditions, see Sec. II B. Moreover, one can distinguish two different setups where the external magnetic field is applied either to the sample only or to the whole device including the leads. In all these cases we can find an analytic expression for u_ϑ , which can be substituted into of Eq. (13c) to find the electric field in the sample, E_r (the radial component of the current is determined by the continuity equation alone). Similarly, Eq. (13d) determines $\delta j_{I\vartheta}$. Using the obtained electric field we can determine the voltage drop through the bulk of the sample as

$$U = \int_{r_1}^{r_2} E_r dr = \int_{r_1}^{r_2} dr \left(\frac{\tilde{R} I}{2\pi r} - \frac{B}{c} u_\vartheta \right). \quad (15)$$

For the no-slip boundary condition for u_ϑ and allowing the external magnetic field to penetrate the leads, the tangential component of the velocity is given by

$$\begin{aligned} u_\vartheta &= -\frac{BI \ell_G^2}{2\pi c \eta r} + \frac{BI (\eta \ell_L^2 - \eta_L \ell_G^2)}{2\pi c \eta \eta_L r_1 r_2} \times \\ &\times \left[K_1 \left(\frac{r}{\ell_G} \right) \frac{r_1 I_1 \left(\frac{r_1}{\ell_G} \right) - r_2 I_1 \left(\frac{r_2}{\ell_G} \right)}{K_1 \left(\frac{r_1}{\ell_G} \right) I_1 \left(\frac{r_2}{\ell_G} \right) - I_1 \left(\frac{r_1}{\ell_G} \right) K_1 \left(\frac{r_2}{\ell_G} \right)} \right. \\ &\quad \left. + I_1 \left(\frac{r}{\ell_G} \right) \frac{r_2 K_1 \left(\frac{r_2}{\ell_G} \right) - r_1 K_1 \left(\frac{r_1}{\ell_G} \right)}{K_1 \left(\frac{r_1}{\ell_G} \right) I_1 \left(\frac{r_2}{\ell_G} \right) - I_1 \left(\frac{r_1}{\ell_G} \right) K_1 \left(\frac{r_2}{\ell_G} \right)} \right], \end{aligned} \quad (16)$$

where η_L is the disorder-induced viscosity [96] and $\ell_L^2 = v_g^2 \eta_L \tau_L / (2P_L)$ is the Gurzhi length in the leads.

In the limit $\ell_G \gg r_1, r_2$ (i.e., “clean system” with long mean free time $\tau_{\text{dis}} \rightarrow \infty$) this simplifies to ($p = r_2/r_1$)

$$u_\vartheta \approx -\frac{BI\ell_L^2}{4\pi c r \eta_L} \left[2 + \left(\frac{1}{\ell_G^2} - \frac{\eta_L}{\eta \ell_L^2} \right) \times \frac{r^2 \ln\left(\frac{r}{r_1}\right) + r^2 p^2 \ln\left(\frac{r_2}{r}\right) - r_2^2 \ln p}{1-p^2} \right]. \quad (17)$$

The corresponding voltage drop remains finite

$$U \approx \left(1 - \frac{\eta \ell_L^2}{\eta_L \ell_G^2} \right) \frac{B^2 I r_2^2}{4\pi c^2 \eta} \frac{(p^2 - 1)^2 - 4p^2 \ln^2 p}{4p^2(p^2 - 1)} + \frac{I \ln p}{2\pi} \left(\frac{B^2 v_g^2 \tau_L}{c^2 3P_L} + \tilde{R} \right), \quad (18a)$$

yielding the field-dependent bulk resistance ($R = U/I$)

$$R(B) \approx \frac{\ln p}{2\pi} R_0 + \frac{B^2 r_2^2}{4\pi c^2 \eta} \frac{(p^2 - 1)^2 - 4p^2 \ln^2 p}{4p^2(p^2 - 1)} + \frac{B^2 v_g^4 \ln p}{2c^2 T^3} \left[\frac{\alpha_1^2 \delta_I}{8 \ln^3 2} \frac{1}{\tau_{\text{dis}}^{-1} + \delta_I^{-1} \tau_{22}^{-1}} + \frac{T^3}{\mu^3} \tau_L \right], \quad (18b)$$

assuming $\eta \ell_L^2 / (\eta_L \ell_G^2) = 3P_L \tau_L / (2P_L \tau_{\text{dis}}) \ll 1$ with $P_L = \mu_L^3 / (3\pi v_g^2)$. The two field-dependent terms differ in their dependence on temperature, sample size, and coupling constant [35] opening a possibility to separate the two contributions from the experimental data and thus to measure the viscosity coefficient.

If the magnetic field is applied to the sample only (and not to the leads) u_ϑ vanishes in the leads and hence the terms with ℓ_L do not appear in the voltage drop (18). In that case, the field-dependent contribution to U does not contain τ_{dis} in contrast to the known result in the strip geometry [23, 30].

A similar result can be obtained in the case of no-stress boundary conditions, where the tangential component of the velocity u_ϑ is still expressed in terms of the Bessel functions. In the clean limit ($\ell_G \gg r_1, r_2$) the voltage drop also remains finite

$$U \approx \frac{I}{2\pi} \left(\tilde{R} + \frac{B^2 \ell_L^2}{c^2 \eta} - \frac{B \eta_H}{e c \eta m_L} \right) \ln p + \frac{r_2^2 B^2 I}{4\pi c^2 \eta} \left[\frac{(p^2 - 1)(p^4 + 10p^2 + 1)}{12p^2(p^2 + 1)^2} - \frac{\ln p}{1 + p^2} \right] + \frac{I}{2\pi} \left[\frac{B^2 (\ell_G^2 - \ell_L^2)}{c^2} + \frac{B \eta_H}{e c \eta m_L} \right] \frac{p^2 - 1}{p^2 + 1}, \quad (19)$$

where η_H is the Hall viscosity in the leads, which vanishes if the magnetic field is not allowed in the leads. In that case, the last term in the voltage drop (19) is proportional

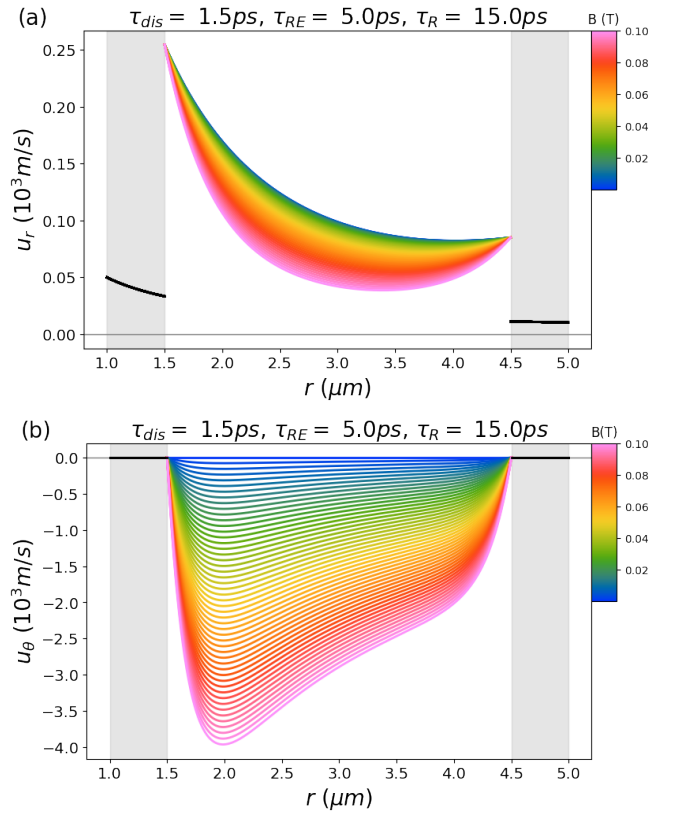


FIG. 3. Radial (top panel) and tangential (bottom panel) components of the hydrodynamic velocity \mathbf{u} computed within the “supercollisions model” of energy relaxation. Black lines in the shaded regions show the drift velocity in the leads. Color curves correspond to different values of the external magnetic field according to the shown color coding. The top curve shows values at $\mathbf{B} = 0$ and is identical with the results of Ref. [65]. For the parameter values, see Fig 1.

to τ_{dis} and independent of viscosity. The second term in Eq. (19) remains similar to Eq. (18) and is inverse proportional to η . This term’s dependence on the ratio p is distinct from both Eq. (18) and the third term in Eq. (19) and could be extracted by analyzing the data in a set of Corbino disks with different p .

In the opposite limit $\ell_G \ll r_1, r_2$, the leading contribution to the bulk voltage drop is independent of η . For no-slip boundary conditions and in the simplified case where the field is not allowed to penetrate the leads we find for the field-dependent part of U

$$R(B) - R(0) \approx \frac{B^2 v_g^2 \tau_{\text{dis}} \ln p}{6\pi c^2 P} + \frac{\ln p}{2\pi} \delta_I \alpha_1^2 \tilde{R}_B \propto \tau_{\text{dis}} B^2. \quad (20)$$

The voltage drop (20) is proportional to τ_{dis} similarly to the result in the strip geometry (see Refs. [23, 30]). Of course, in the limit $\ell_G \ll r_1, r_2$ the mean free time τ_{dis} cannot be arbitrarily large, hence the voltage drop (20) does not diverge. In the limit $\tau_{\text{dis}} \rightarrow \infty$ the voltage drop crosses over to the above “clean” limit and is given by Eq. (18). However, the limiting expression (20) is

independent of viscosity, and hence qualitatively similar to the usual result.

To summarize the results of this section, we have shown that bulk magnetoresistance in neutral graphene in the Corbino geometry exhibits a crossover between the “clean” limit of the large (compared to the disk radius) Gurzhi length to the limit of small Gurzhi length. In the former case, the field-dependent part of the bulk voltage drop is determined by viscosity, while in the latter limit it is proportional to the disorder mean free time similarly to the known result in the strip geometry.

B. Radial component of the velocity and the device resistance

The five equations (14) can be reduced to two coupled differential equations (for similar calculations in the strip geometry see Refs. [23, 48, 68, 82]). To simplify the arguments, we introduce the following notations

$$q = n_I u_r, \quad p = \delta j_{I,r}, \quad x = \frac{2n_I}{3P} \delta P, \quad y = \frac{12 \ln 2}{\pi^2} \frac{n_I}{T} \mu_I. \quad (21)$$

In terms of the new variables, Eqs. (14a) and (14c) can be written as

$$\frac{1}{r} \frac{\partial(rq)}{\partial r} + \frac{1}{r} \frac{\partial(rp)}{\partial r} = -\frac{y}{\tau_R}, \quad (22a)$$

$$\frac{1}{r} \frac{\partial(rq)}{\partial r} = -\frac{x}{\tau_{RE}}. \quad (22b)$$

Equation (14e) can be rewritten as

$$\frac{\partial y}{\partial r} = -\frac{6}{\pi} \frac{\tilde{R} n_I}{R_0 T^2 \tilde{\tau}} p - \frac{12 \ln 2}{\pi} \frac{\alpha_1 \omega_B^2}{e^2 v_g^2 R_0 T} q, \quad (23a)$$

where $\tilde{\tau} = \delta_I / (\tau_{\text{dis}}^{-1} + \delta_I^{-1} \tau_{22}^{-1})$. Finally, Eqs. (14b) and (14d) can be combined into

$$\begin{aligned} \frac{\partial x}{\partial r} = & \frac{2\eta}{3P} \frac{\partial}{\partial r} \frac{1}{r} \frac{\partial(rq)}{\partial r} - \frac{2}{v_g^2} \left[\tau_{\text{dis}}^{-1} + \frac{\omega_B^2}{e^2 \tilde{R}} \frac{4T^2 \ln^2 2}{3P v_g^2} \right] q \\ & + \alpha_1 \tilde{\tau} \frac{\pi^2 T^2}{9P v_g^2} \frac{\omega_B^2}{e^2 \tilde{R}} \frac{\partial y}{\partial r}. \end{aligned} \quad (23b)$$

Introducing the differential operator

$$\hat{\mathbb{D}}q = \frac{\partial}{\partial r} \frac{1}{r} \frac{\partial(rq)}{\partial r}, \quad (24)$$

we rewrite Eqs. (22) in the matrix form

$$\hat{\mathbb{D}} \begin{pmatrix} q \\ p \end{pmatrix} = \hat{T}_S \begin{pmatrix} \partial x / \partial r \\ \partial y / \partial r \end{pmatrix}, \quad \hat{T}_S = \begin{pmatrix} \frac{1}{\tau_{RE}} & 0 \\ -\frac{1}{\tau_{RE}} & \frac{1}{\tau_R} \end{pmatrix}. \quad (25a)$$

Similarly, Eqs. (23) can be written in the matrix form

$$\begin{pmatrix} \partial x / \partial r \\ \partial y / \partial r \end{pmatrix} = -\hat{M} \begin{pmatrix} q \\ p \end{pmatrix} + \hat{V} \hat{\mathbb{D}} \begin{pmatrix} q \\ p \end{pmatrix}, \quad (25b)$$

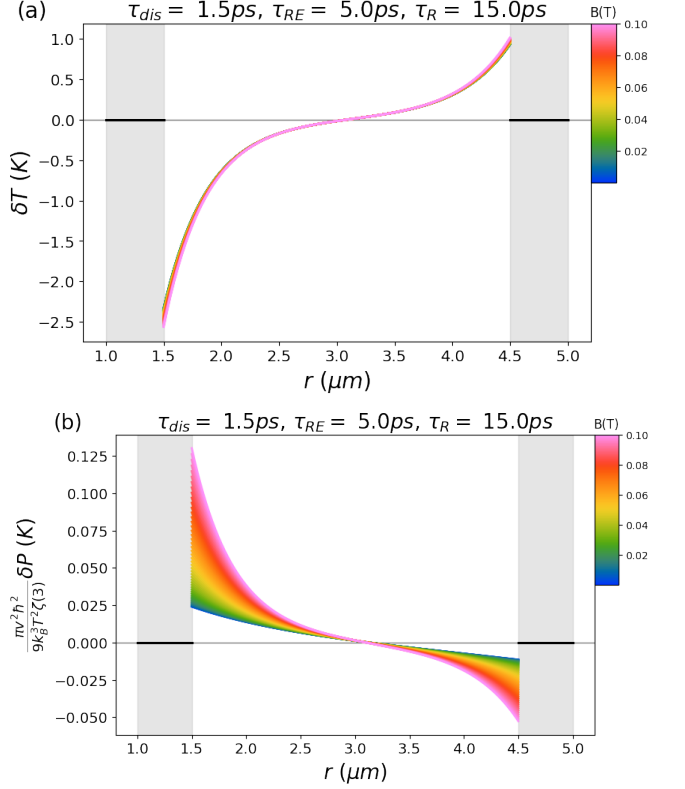


FIG. 4. Local variations of temperature (top panel) and pressure (bottom panel) in the Corbino device computed within the “supercollisions model” of energy relaxation. Black lines in the shaded regions indicate that the leads are at equilibrium. Color curves correspond to different values of the external magnetic field according to the shown color coding. Zero field values are identical with the results of Ref. [65]. For the parameter values, see Fig 1.

where

$$\hat{V} = \begin{pmatrix} \frac{2\eta}{3P} & 0 \\ 0 & 0 \end{pmatrix},$$

and

$$\hat{M} = \begin{pmatrix} \frac{16 \ln^3 2}{3\pi} \frac{\delta_I \tilde{R}_B T^3}{v_g^4 P R_0 \tilde{\tau}} + \frac{2}{v_g^2 \tau_{\text{dis}}} & \frac{4 \ln 2}{3} \frac{\alpha_1 \delta_I n_I \tilde{R}_B T}{v_g^2 P R_0 \tilde{\tau}} \\ \frac{24 \ln^2 2}{\pi^2} \frac{\alpha_1 \delta_I \tilde{R}_B}{v_g^2 R_0 \tilde{\tau}} & \frac{6}{\pi} \frac{n_I \tilde{R}}{R_0 T^2 \tilde{\tau}} \end{pmatrix}.$$

Finally, combining Eqs. (25) we find the equation for the variables p and q

$$\hat{\mathbb{D}} \begin{pmatrix} q \\ p \end{pmatrix} = \hat{K} \begin{pmatrix} q \\ p \end{pmatrix}, \quad \hat{K} = [1 - \hat{T}_S \hat{V}]^{-1} \hat{T}_S \hat{M}. \quad (26)$$

The obtained equation should be solved with the boundary conditions (9). The solution is straightforward albeit tedious. The results can be expressed in terms of linear combinations of the Bessel functions. Thus obtained solutions are not particularly instructive, hence we present the results of the calculation in graphical form.

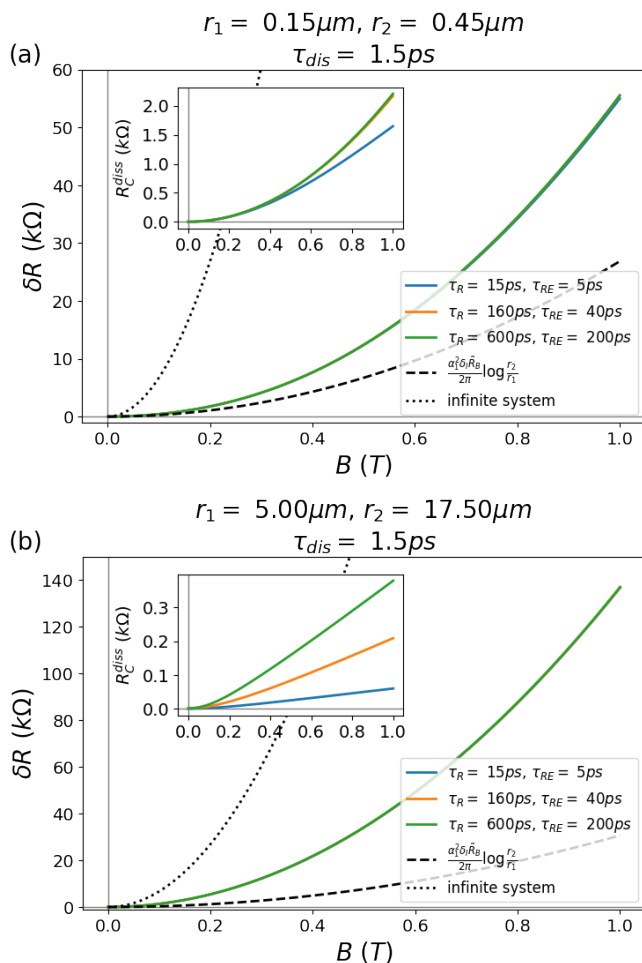


FIG. 5. Magnetoresistance of a small (top panel) and large (bottom panel) Corbino device computed within the “supercollisions model” of energy relaxation. The radii of the Corbino disks are shown above the plots. The black dotted line shows the quantity \hat{R} , which is of the same order of magnitude as the magnetoresistance in the infinite system [23, 82]. Color curves correspond to three different sets of values of the relaxation times. For other parameter values (yielding $\ell_G = 0.2 \mu\text{m}$), see Fig. 1. The insets show the contact resistance due to viscous dissipation.

The radial component of the hydrodynamic velocity is shown in the top panel of Fig. 3. The drift velocity in the leads shows the standard Corbino profile, $u_r \propto 1/r$. At each interface, u_r exhibits a jump due to the mismatch of the entropy densities in the sample and leads. For high enough magnetic field, u_r has a sign change close to the interface. However, the corresponding change of direction is hardly seen in the overall flow diagram shown in Fig. 1, since the numerical value of the tangential component u_θ is much larger (see the bottom panel of Fig. 3).

The hydrodynamic velocity determines the energy current in the system. The nonuniform energy current results in local variations of the electronic temperature from its equilibrium value (see Fig. 4). The inhomoge-

neous temperature profile suggests that energy relaxation is less effective in strong magnetic fields. Fig. 1 shows the same data as Fig. 4 but in the form of the color map.

Finally we use the boundary conditions (12) to find the interface jumps of the electric potential which allows us to determine the device resistance. The procedure is the same as in the case of $\mathbf{B} = 0$ discussed in Ref. [65]. The results are shown in Fig. 5. For small enough samples (see the top panel in Fig. 5) the device resistance deviates only slightly from \hat{R} which is of the same order of magnitude as the magnetoresistance in the infinite system [23, 82]. In large samples the deviation is more pronounced and depends on the actual radius of the disk rather than on the ratio p (which is the same in both plots).

The quantitative results shown in this section were computed for a particular choice of the relaxation times. These values are largely phenomenological; however, the magnetoresistance shown in Fig. 5 hardly depends on them, while for larger samples (the bottom panel) the three curves are indistinguishable. However, the values of the relaxation times cannot be completely arbitrary. The point is that the matrix \hat{K} in Eq. (26) is not guaranteed to have real, positive eigenvalues (although its determinant is positive). In particular, the recombination time τ_R and energy relaxation time τ_{RE} cannot be very different. Within the physical model of supercollisions [59] these time-scales are of the same order of magnitude. Quasiparticle recombination involves supercollision scattering between the bands, while energy relaxation includes an additional contribution of intraband scattering. As a result, the energy relaxation time is shorter than τ_R , but not much shorter since the model does not involve any additional parameter. For such physical values of the relaxation times the eigenvalues of the matrix \hat{K} are real positive and the resulting magnetoresistance is well accounted for by the curves shown in Fig. 5 where, again, the particular values of τ_R and τ_{RE} do not have a strong quantitative impact on the overall resistance magnitude.

C. Energy relaxation due to electron-phonon interaction

Supercollisions are scattering events involving electron scattering off a phonon and an impurity. As such, this is a next-order process as compared to the direct electron-phonon scattering. The reason supercollisions might be important is that the speed of sound is much smaller than v_g . At high enough temperatures [59, 60] supercollisions indeed dominate, but at lower temperatures the direct electron-phonon scattering cannot be neglected.

Energy relaxation and quasiparticle recombination due to electron-phonon scattering was considered in Ref. [23] within the linear response theory. Since the macroscopic equations of the linear response theory coincide with the linearized hydrodynamic equations [22], we can directly incorporate the corresponding decay terms into our hydrodynamic theory. These decay terms appear in

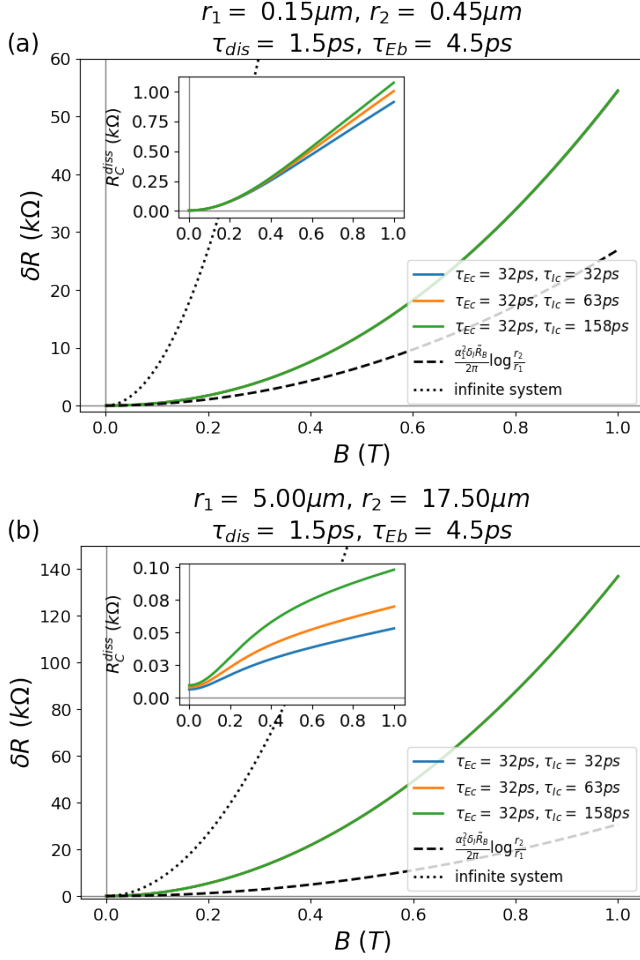


FIG. 6. Magnetoresistance in small (top) and large (bottom) Corbino devices computed within the “electron-phonon model” of energy relaxation (cf. Fig. 5).

Eq. (25a) through the matrix \hat{T}_S . The model of electron-phonon interaction introduced in Ref. [23] corresponds to the following choice of this matrix

$$\hat{T}_{ep} = -\frac{1}{|\Delta|} \begin{pmatrix} \frac{\gamma}{\tau_{Ec}} + \frac{1}{\tau_{Eb}} & -\frac{\gamma^2}{\mathcal{N}_2 \tau_{Eb}} - \frac{\gamma}{\tau_{Ec}} \\ -\frac{\gamma^2 \mathcal{N}_2}{\gamma \tau_{Ec}} - \frac{\mathcal{N}_2}{\tau_{Ic}} - \frac{1}{\tau_{Eb}} & \frac{2\gamma}{\tau_{Ec}} + \frac{\gamma^2}{\mathcal{N}_2 \tau_{Eb}} + \frac{\mathcal{N}_2}{\tau_{Ic}} \end{pmatrix}, \quad (27)$$

where

$$\gamma = \frac{\pi^2}{12 \ln^2 2}, \quad \mathcal{N}_2 = \frac{9\zeta(3)}{8 \ln^3 2}, \quad \Delta = \gamma^2 - \mathcal{N}_2,$$

and $\tau_{Eb} \ll \tau_{Ec} \leq \tau_{Ic}$ describe the three independent components of the electron-phonon collision integral [23].

Repeating the above calculation with \hat{T}_{ep} instead of \hat{T}_S , we arrive at the results that are largely similar to those obtained within the supercollision model, but with a few notable differences (see Figs. 6-11). Unless specified in the figure captions, the parameter values used for the quantitative computation are the same as in the case of supercollisions (see the caption to Fig. 1).

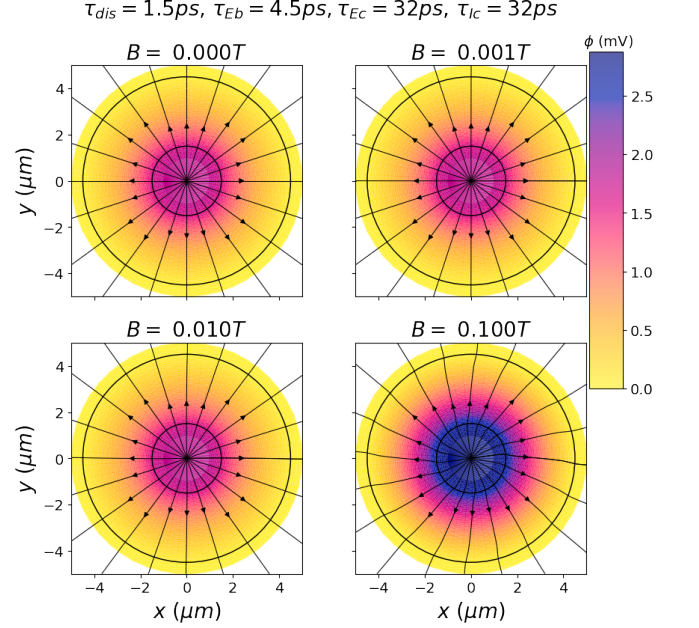


FIG. 7. Electric current density \mathbf{j} and potential ϕ within the electron-phonon model of energy relaxation (cf. Fig. 2).

Magnetoresistance of the device is still positive and parabolic (see Fig. 6). In small devices, it is still largely determined by the quantity \tilde{R} (shown by the black dotted line in Fig. 6 similarly to Fig. 5). In this case, variations of the electron-phonon relaxation rates still do not affect the result in any noticeable way. The results for large devices are also similar to the case of supercollisions: calculated magnetoresistance clearly exceeds \tilde{R} and thus shows a strong dependence on the size of the device (but not on the ratio p).

The electric current density and potential in the device are seen largely the same as in the case of supercollisions, although the deviation of the current from the radial direction (i.e., its tangential component δj_θ) is somewhat smaller (see Fig. 7, cf. Fig. 2). This result seems to be consistent with the similarities in the magnetoresistance in the two cases.

The hydrodynamic velocity \mathbf{u} is still dominated by its tangential component (see Figs. 8 and 9). The latter shows the behavior that is largely similar to that shown in the bottom panel of Fig. 3, although the magnitude of u_θ shows stronger growth with increasing magnetic field. In contrast, the temperature variation is “reversed”: now the electronic temperature is increased around the inner contact and decreased close to the outer one (the opposite behavior to that seen in Figs. 1 and 4) (see Fig. 10).

The reversed behavior of the temperature variation corresponds to the change in the radial component of the hydrodynamic velocity u_r . While the jumps at the interfaces with the leads remain the same (insofar u_r on the sample side of the interface is larger than the drift velocity in the leads), the initial slope of u_r as a function

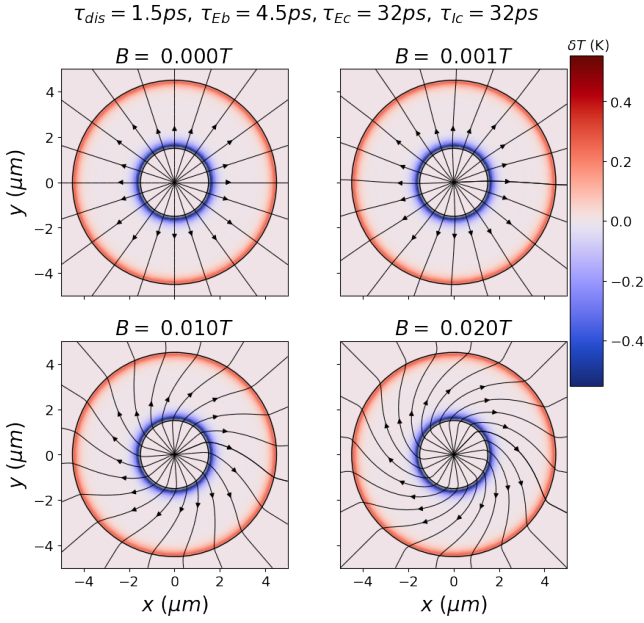


FIG. 8. Hydrodynamic velocity \mathbf{u} and temperature δT distribution in the device obtained by solving the hydrodynamic equations at relatively low temperatures where energy relaxation is dominated by direct electron-phonon scattering (cf. Fig. 1).

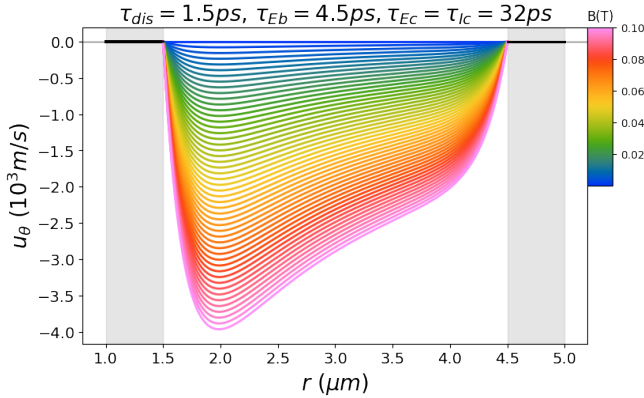


FIG. 9. Tangential component of the hydrodynamic velocity u_θ computed within the “electron-phonon model” of energy relaxation (cf. Fig. 3).

of the radial coordinate has the opposite sign, which does not change with the increase in the magnetic field.

Overall, it is rather natural that the choice of the energy relaxation model mostly affects the energy flow in the device rather than the charge flow. This is a clear consequence of the decoupling of the energy and electric currents in neutral graphene. Although the two currents are being coupled by the magnetic field, the effect appears to be subleading. It is not surprising that the effect of this coupling is most pronounced in strong magnetic fields and large Corbino disks.

Contact resistance induced by viscous dissipation (see

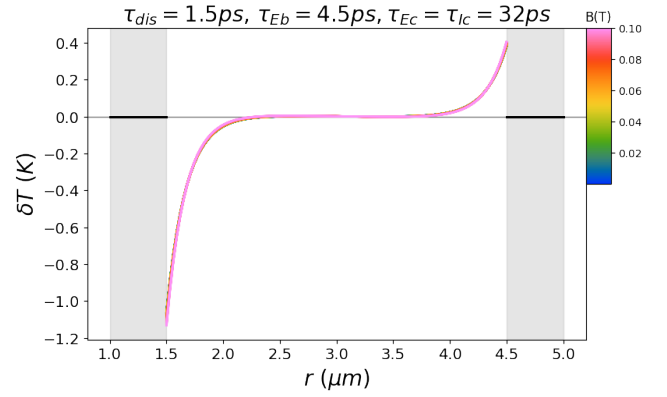


FIG. 10. Local temperature variation computed within the “electron-phonon model” of energy relaxation (cf. Fig. 3).

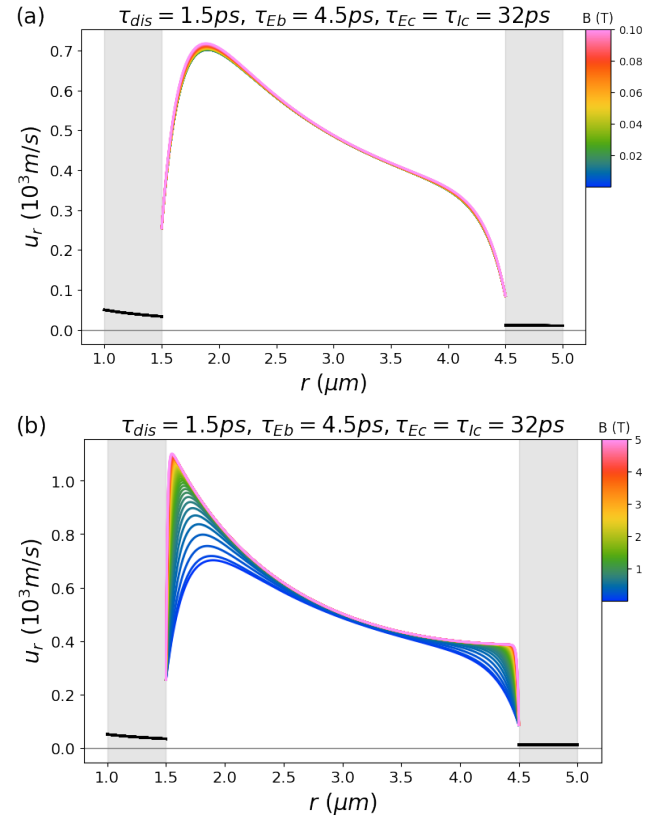


FIG. 11. Radial component of the hydrodynamic velocity u_r computed within the “electron-phonon model” of energy relaxation (cf. Fig. 3).

insets in Figs. 5 and 6) is also affected by the choice of the energy relaxation model. In the case of supercollisions its qualitative behavior exhibits a strong dependence on the size of the disk (see Fig. 5), while in the model of electron-phonon scattering this dependence is reduced to the magnitude only. The contact resistance is significantly stronger in small devices for both choices of the energy relaxation model as expected on general grounds.

IV. SUMMARY

In this paper we considered hydrodynamic flows of charge and energy in neutral graphene Corbino disks. We have shown that the Corbino geometry offers a (in principle realizable) possibility to measure electronic viscosity in neutral graphene, a task that so far has appeared elusive. The viscosity coefficient could be extracted from the magnetoresistance data in the ultra-clean limit where the bulk contribution to the device resistance is independent of the electron-impurity scattering time. The bulk resistance dominates over the contact resistance for larger sized disks and hence can in principle be measured in laboratory experiments.

Corbino magnetoresistance in graphene is illustrated in Figs. 5 and 6, where the calculated magnetoresistance is shown for two models of energy relaxation. In both cases, the dependence $R(B)$ is parabolic, similarly to the known result in the strip geometry. The viscosity coefficient can be *in principle* determined experimentally by analyzing the data in a set of different Corbino disks (see Sec. III A). This is not a straightforward task since the magnetoresistance is given by a sum of viscosity-dependent and viscosity-independent terms. In the clean limit $\ell_G \ll r_1, r_2$ [see Eq. (18)], these terms exhibit distinct dependence on the sample size r_2 , the ratio of the radii $p = r_2/r_1$, and temperature, making it possible to extract the viscosity coefficient from the experimental data. In the opposite limit [see Eq. (19)], the dominant contribution to magnetoresistance is independent of viscosity. Existing experiments appear to be in the crossover between these two limits. In this paper we have used parameter values yielding $\ell_G \approx 0.2 \mu\text{m}$. The size of the Corbino disk used in a recent experiment [31] was $r_1 = 2 \mu\text{m}$, $r_2 = 9 \mu\text{m}$, which is closer to the “large Corbino disk” illustrated in panels (b) in Figs. 5 and 6 than to the clean limit. It is fair to say that at present extracting viscosity from Corbino magnetoresistance measurements would be extremely difficult. At the same time, we are not aware of any other way to measure

the viscosity coefficient in neutral graphene. We believe that viscosity measurements and more generally experimental observation of purely viscous effects in neutral graphene will be more accessible in the near future with even cleaner samples (increasing τ_{dis} by an order of magnitude).

The regime of linear magnetoresistance as seen in the strip geometry or infinitely sized models does not exist in the Corbino geometry. This can be easily understood by noting that the origin of linear magnetoresistance is in the accumulation of energy and quasiparticle density in the boundary region of a long strip where the sample edges provide a natural barrier for the lateral neutral flow of quasiparticles induced by the magnetic field. In a Corbino disk there is no such edge. The lateral currents (energy and imbalance) flow freely around the disk without accumulating quasiparticles at any point.

Unlike the case of a single-band conductor (e.g., doped graphene), at charge neutrality the electric field is not expelled from the bulk of the sample. Nevertheless bulk viscous dissipation does lead to a discontinuity of the electric potential at the sample-lead interfaces inducing an additional contact resistance. This resistance however is rather small as compared to the resistance of the whole device and should not have a strong effect on the viscosity measurements.

ACKNOWLEDGMENTS

The authors are grateful to P. Hakonen, V. Kachorovskii, A. Levchenko, A. Mirlin, J. Schmalian, A. Shnirman, and M. Titov for fruitful discussions. This work was supported by the German Research Foundation DFG within FLAG-ERA Joint Transnational Call (Project GRANSPORE), by the European Commission under the EU Horizon 2020 MSCA-RISE-2019 Program (Project No. 873028 HYDROTRONICS), by the German Research Foundation DFG project NA 1114/5-1 (B.N.N.), and by the German-Israeli Foundation for Scientific Research and Development (GIF) Grant No. I-1505-303.10/2019 (I.V.G.).

-
- [1] M. Polini and A. K. Geim, *Phys. Today* **73**, 28 (2020).
 [2] B. N. Narozhny, *Riv. Nuovo Cim.* **45**, 661–736 (2022).
 [3] A. Lucas and K. C. Fong, *J. Phys: Condens. Matter* **30**, 053001 (2018).
 [4] B. N. Narozhny, I. V. Gornyi, A. D. Mirlin, and J. Schmalian, *Annalen der Physik* **529**, 1700043 (2017).
 [5] D. A. Bandurin, I. Torre, R. Krishna Kumar, M. Ben Shalom, A. Tomadin, A. Principi, G. H. Auton, E. Khestanova, K. S. Novoselov, I. V. Grigorieva, et al., *Science* **351**, 1055 (2016).
 [6] A. I. Berdyugin, S. G. Xu, F. M. D. Pellegrino, R. Krishna Kumar, A. Principi, I. Torre, M. B. Shalom, T. Taniguchi, K. Watanabe, I. V. Grigorieva, et al., *Science* **364**, 162 (2019).
 [7] M. J. H. Ku, T. X. Zhou, Q. Li, Y. J. Shin, J. K. Shi, C. Burch, L. E. Anderson, A. T. Pierce, Y. Xie, A. Hamo, et al., *Nature* **583**, 537 (2020).
 [8] J. A. Sulpizio, L. Ella, A. Rozen, J. Birkbeck, D. J. Perello, D. Dutta, M. Ben-Shalom, T. Taniguchi, K. Watanabe, T. Holder, et al., *Nature* **576**, 75 (2019).
 [9] R. Krishna Kumar, D. A. Bandurin, F. M. D. Pellegrino, Y. Cao, A. Principi, H. Guo, G. H. Auton, M. Ben Shalom, L. A. Ponomarenko, G. Falkovich, et al., *Nat. Phys.* **13**, 1182 (2017).
 [10] A. Jenkins, S. Baumann, H. Zhou, S. A. Meynell, D. Yang, T. T. K. Watanabe, A. Lucas, A. F. Young,

- and A. C. Bleszynski Jayich (2020), arXiv:2002.05065.
- [11] J. Mayzel, V. Steinberg, and A. Varshney, *Nat. Commun.* **10**, 937 (2019).
- [12] I. Matthaïakakis, D. Rodríguez Fernández, C. Tutschku, E. M. Hankiewicz, J. Erdmenger, and R. Meyer, *Phys. Rev. B* **101**, 045423 (2020).
- [13] P. Rao and B. Bradlyn, *Phys. Rev. X* **10**, 021005 (2020).
- [14] R. Cohen and M. Goldstein, *Phys. Rev. B* **98**, 235103 (2018).
- [15] P. K. Kovtun, D. T. Son, and A. O. Starinets, *Phys. Rev. Lett.* **94**, 111601 (2005).
- [16] T. Schäfer, *Annu. Rev. Nucl. Part. Sci.* **64**, 125 (2014).
- [17] J. Zaanen, *Nat. Phys.* **9**, 609 (2013).
- [18] K. Kaushansky, M. A. Lichtman, J. T. Prchal, M. Levi, L. J. Burns, and D. C. Linch, eds., *Williams Hematology* (McGraw Hill, New York, 2021).
- [19] R. N. Gurzhi, *Soviet Physics Uspekhi* **11**, 255 (1968), [*Usp. Fiz. Nauk* **94**, 689 (1968)].
- [20] L. S. Levitov and G. Falkovich, *Nat. Phys.* **12**, 672 (2016).
- [21] U. Briskot, M. Schütt, I. V. Gornyi, M. Titov, B. N. Narozhny, and A. D. Mirlin, *Phys. Rev. B* **92**, 115426 (2015).
- [22] B. N. Narozhny, *Ann. Phys.* **411**, 167979 (2019).
- [23] B. N. Narozhny, I. V. Gornyi, M. Titov, M. Schütt, and A. D. Mirlin, *Phys. Rev. B* **91**, 035414 (2015).
- [24] A. B. Kashuba, *Phys. Rev. B* **78**, 085415 (2008).
- [25] L. Fritz, J. Schmalian, M. Müller, and S. Sachdev, *Phys. Rev. B* **78**, 085416 (2008).
- [26] M. Müller, L. Fritz, and S. Sachdev, *Phys. Rev. B* **78**, 115406 (2008).
- [27] M. Schütt, P. M. Ostrovsky, I. V. Gornyi, and A. D. Mirlin, *Phys. Rev. B* **83**, 155441 (2011).
- [28] B. N. Narozhny, *Phys. Rev. B* **100**, 115434 (2019).
- [29] B. N. Narozhny, I. V. Gornyi, and M. Titov, *Phys. Rev. B* **103**, 115402 (2021).
- [30] M. Müller and S. Sachdev, *Phys. Rev. B* **78**, 115419 (2008).
- [31] C. Kumar, J. Birkbeck, J. A. Sulpizio, D. J. Perello, T. Taniguchi, K. Watanabe, O. Reuven, T. Scaffidi, A. Stern, A. K. Geim, et al., *Nature* **609**, 276 (2022).
- [32] M. J. M. de Jong and L. W. Molenkamp, *Phys. Rev. B* **51**, 13389 (1995).
- [33] U. Vool, A. Hamo, G. Varnavides, Y. Wang, T. X. Zhou, N. Kumar, Y. Dovzhenko, Z. Qiu, C. A. C. Garcia, A. T. Pierce, et al., *Nat. Phys.* **17**, 1216 (2021).
- [34] P. J. W. Moll, P. Kushwaha, N. Nandi, B. Schmidt, and A. P. Mackenzie, *Science* **351**, 1061 (2016).
- [35] M. Kim, S. G. Xu, A. I. Berdyugin, A. Principi, S. Slizovskiy, N. Xin, P. Kumaravadivel, W. Kuang, M. Hamer, R. Krishna Kumar, et al., *Nat. Commun.* **11**, 2339 (2020).
- [36] G. M. Gusev, A. D. Levin, E. V. Levinson, and A. K. Bakarov, *Phys. Rev. B* **98**, 161303(R) (2018).
- [37] G. M. Gusev, A. S. Jaroshevich, A. D. Levin, Z. D. Kvon, and A. K. Bakarov, *Sci. Rep.* **10**, 7860 (2020).
- [38] G. M. Gusev, A. S. Jaroshevich, A. D. Levin, Z. D. Kvon, and A. K. Bakarov, *Phys. Rev. B* **103**, 075303 (2021).
- [39] O. E. Raichev, G. M. Gusev, A. D. Levin, and A. K. Bakarov, *Phys. Rev. B* **101**, 235314 (2020).
- [40] A. Gupta, J. J. Heremans, G. Kataria, M. Chandra, S. Fallahi, G. C. Gardner, and M. J. Manfra, *Phys. Rev. Lett.* **126**, 076803 (2021).
- [41] G. Varnavides, A. S. Jermyn, P. Anikeeva, C. Felser, and P. Narang, *Nat. Commun.* **11**, 4710 (2020).
- [42] J. Gooth, F. Menges, N. Kumar, V. Süß, C. Shekhar, Y. Sun, U. Drechsler, R. Zierold, C. Felser, and B. Gotsmann, *Nature Communications* **9**, 4093 (2018).
- [43] A. Jaoui, B. Fauqué, and K. Behnia, *Nat. Commun.* **12**, 195 (2021).
- [44] I. Torre, A. Tomadin, A. K. Geim, and M. Polini, *Phys. Rev. B* **92**, 165433 (2015).
- [45] P. S. Alekseev, *Phys. Rev. Lett.* **117**, 166601 (2016).
- [46] T. Scaffidi, N. Nandi, B. Schmidt, A. P. Mackenzie, and J. E. Moore, *Phys. Rev. Lett.* **118**, 226601 (2017).
- [47] F. M. D. Pellegrino, I. Torre, and M. Polini, *Phys. Rev. B* **96**, 195401 (2017).
- [48] P. S. Alekseev, A. P. Dmitriev, I. V. Gornyi, V. Y. Kachorovskii, B. N. Narozhny, and M. Titov, *Phys. Rev. B* **97**, 085109 (2018).
- [49] P. S. Alekseev, A. P. Dmitriev, I. V. Gornyi, V. Y. Kachorovskii, B. N. Narozhny, and M. Titov, *Phys. Rev. B* **98**, 125111 (2018).
- [50] T. Holder, R. Queiroz, T. Scaffidi, N. Silberstein, A. Rozen, J. A. Sulpizio, L. Ella, S. Ilani, and A. Stern, *Phys. Rev. B* **100**, 245305 (2019).
- [51] S. S. Pershoguba, A. F. Young, and L. I. Glazman, *Phys. Rev. B* **102**, 125404 (2020).
- [52] S. Danz and B. N. Narozhny, *2D Materials* **7**, 035001 (2020).
- [53] J. L. M. Poiseuille, *C. R. Acad. Sci.* **11**, 961 (1840).
- [54] J. L. M. Poiseuille, *Annales de chimie et de physique (Series 3)* **21**, 76 (1847).
- [55] L. D. Landau and E. M. Lifshitz, *Fluid Mechanics* (Pergamon Press, London, 1987).
- [56] J. M. Link, B. N. Narozhny, E. I. Kiselev, and J. Schmalian, *Phys. Rev. Lett.* **120**, 196801 (2018).
- [57] H.-Y. Xie and M. S. Foster, *Phys. Rev. B* **93**, 195103 (2016).
- [58] H.-Y. Xie and A. Levchenko, *Phys. Rev. B* **99**, 045434 (2019).
- [59] B. N. Narozhny and I. V. Gornyi, *Frontiers in Physics* **9**, 108 (2021).
- [60] J. C. W. Song, M. Y. Reizer, and L. S. Levitov, *Phys. Rev. Lett.* **109**, 106602 (2012).
- [61] M. W. Graham, S.-F. Shi, D. C. Ralph, J. Park, and P. L. McEuen, *Nat. Phys.* **9**, 103 (2013).
- [62] A. C. Betz, S. H. Jhang, E. Pallecchi, R. Ferreira, G. Fève, J.-M. Berroir, and B. Plaçais, *Nat. Phys.* **9**, 109 (2013).
- [63] K. S. Tikhonov, I. V. Gornyi, V. Y. Kachorovskii, and A. D. Mirlin, *Phys. Rev. B* **97**, 085415 (2018).
- [64] J. F. Kong, L. Levitov, D. Halbertal, and E. Zeldov, *Phys. Rev. B* **97**, 245416 (2018).
- [65] V. Gall, B. N. Narozhny, and I. V. Gornyi, *Phys. Rev. B* **107**, 045413 (2023).
- [66] M. Titov, R. V. Gorbachev, B. N. Narozhny, T. Tudorovskiy, M. Schütt, P. M. Ostrovsky, I. V. Gornyi, A. D. Mirlin, M. I. Katsnelson, K. S. Novoselov, et al., *Phys. Rev. Lett.* **111**, 166601 (2013).
- [67] P. S. Alekseev, A. P. Dmitriev, I. V. Gornyi, V. Y. Kachorovskii, B. N. Narozhny, M. Schütt, and M. Titov, *Phys. Rev. Lett.* **114**, 156601 (2015).
- [68] P. S. Alekseev, A. P. Dmitriev, I. V. Gornyi, V. Y. Kachorovskii, B. N. Narozhny, M. Schütt, and M. Titov, *Phys. Rev. B* **95**, 165410 (2017).

- [69] G. Y. Vasileva, D. Smirnov, Y. L. Ivanov, Y. B. Vasilyev, P. S. Alekseev, A. P. Dmitriev, I. V. Gornyi, V. Y. Kachorovskii, M. Titov, B. N. Narozhny, et al., Phys. Rev. B **93**, 195430 (2016).
- [70] O. M. Corbino, Nuovo Cimento **1**, 397 (1911).
- [71] A. Tomadin, G. Vignale, and M. Polini, Phys. Rev. Lett. **113**, 235901 (2014).
- [72] T. Holder, R. Queiroz, and A. Stern, Phys. Rev. Lett. **123**, 106801 (2019).
- [73] M. Shavit, A. V. Shtyov, and G. Falkovich, Phys. Rev. Lett. **123**, 026801 (2019).
- [74] A. Hui, V. Oganessian, and E.-A. Kim, Phys. Rev. B **103**, 235152 (2021).
- [75] S. Li, A. Levchenko, and A. V. Andreev, Phys. Rev. B **105**, 125302 (2022).
- [76] A. Stern, T. Scaffidi, O. Reuven, C. Kumar, J. Birkbeck, and S. Ilani (2021), arXiv:2110.15369.
- [77] O. E. Raichev (2022), arXiv:2202.06623.
- [78] A. Levchenko, S. Li, and A. V. Andreev, Phys. Rev. B **106**, L201306 (2022).
- [79] B. N. Narozhny and M. Schütt, Phys. Rev. B **100**, 035125 (2019).
- [80] B. N. Narozhny, Annals of Physics **454**, 169341 (2023).
- [81] M. S. Foster and I. L. Aleiner, Phys. Rev. B **79**, 085415 (2009).
- [82] B. N. Narozhny, I. V. Gornyi, and M. Titov, Phys. Rev. B **104**, 075443 (2021).
- [83] M. Müller, J. Schmalian, and L. Fritz, Phys. Rev. Lett. **103**, 025301 (2009).
- [84] D. E. Sheehy and J. Schmalian, Phys. Rev. Lett. **99**, 226803 (2007).
- [85] J. González, F. Guinea, and M. A. H. Vozmediano, Phys. Rev. B **59**, R2474 (1999).
- [86] J. Gonzalez, F. Guinea, and M. A. H. Vozmediano, Nuclear Physics B **424**, 595 (1994).
- [87] B. N. Narozhny, M. Titov, I. V. Gornyi, and P. M. Ostrovsky, Phys. Rev. B **85**, 195421 (2012).
- [88] M. S. Steinberg, Phys. Rev. **109**, 1486 (1958).
- [89] E. I. Kiselev and J. Schmalian, Phys. Rev. B **99**, 035430 (2019).
- [90] M. P. Marder, *Condensed Matter Physics* (Wiley, 2010).
- [91] M. Kamada, V. Gall, J. Sarkar, M. Kumar, A. Laitinen, I. Gornyi, and P. Hakonen, Phys. Rev. B **104**, 115432 (2021).
- [92] M. Kumar, A. Laitinen, and P. Hakonen, Nature Communications **9**, 2776 (2018).
- [93] B. L. Altshuler and A. G. Aronov, in *Electron-Electron Interactions in Disordered Systems*, edited by A. L. Efros and M. Pollak (North-Holland, Amsterdam, 1985).
- [94] G. Zala, B. N. Narozhny, and I. L. Aleiner, Phys. Rev. B **64**, 214204 (2001).
- [95] B. N. Narozhny, I. L. Aleiner, and A. Stern, Phys. Rev. Lett. **86**, 3610 (2001).
- [96] I. S. Burmistrov, M. Goldstein, M. Kot, V. D. Kurilovich, and P. D. Kurilovich, Phys. Rev. Lett. **123**, 026804 (2019).